# Radiolabeled Cobaltabisdicarbollide Anion-Graphene Oxide Nanocomposites for In-Vivo Bioimaging and Boron Delivery

Albert Ferrer-Ugalde,[a] Stefania Sandoval,[a] Krishna Reddy Pulagam,[b] Amanda Muñoz-Juan,[a] Anna Laromaine,[a] Jordi Llop,[b] Gerard Tobias,*[a] and Rosario Núñez*[a]

*[a] Institut de Ciència de Materials de Barcelona, ICMAB-CSIC, Campus UAB 08193, Bellaterra, Spain.*

*[b] CICbiomaGUNE, Basque Research and Technology Alliance (BRTA), Paseo de Miramón 182, 20014 Donostia, San Sebastián, Spain.*

Corresponding Authors: Rosario Núñez and Gerard Tobias. Institut de Ciència de Materials de Barcelona, ICMAB-CSIC, Campus UAB, 08193 Bellaterra, Barcelona, Spain. Tel.: +34 93 580 1853. Fax: +34 93 580 5729. rosario@icmab.es; gerard.tobias@icmab.es

**Abstract**

A carbon-based hybrid nanocomposite, which consists of monoiodinated boron-cluster derivatives covalently attached to graphene oxide, is hereby introduced. This **GO-I-COSAN** has been synthesized using a novel boron-rich cobaltabisdicarbollide precursor with one iodide group attached to one of the boron atoms of the cluster (**I-COSAN**), and designed to be subsequently labeled with radioactive $^{124}$I for its use in Positron Emission Tomography (PET). *In-vitro* cytotoxicity studies of **GO-I-COSAN** with HeLa cells at different concentrations up to 48 h proved that the cell mortality was lower than 10 %, indicating minimal cytotoxicity of the nanomaterial. Remarkably, the internalization of the nanomaterial by cells was confirmed by Transmission Electron Microscopy (TEM), which indicated its accumulation in the cytoplasm, without causing changes neither in the size nor in the morphology of cells. Additionally, *in vivo* tests using C. *elegans* confirmed that **GO-I-COSAN** could be ingested by the worms, showing no significant damage and very low toxicity, which supports the results observed in the *in-vitro* studies. Radioisotopic labeling of **I-COSAN** using a Pd-catalyzed isotopic exchange reaction with Na[$^{124}$I]I and its subsequent functionalization onto **GO** was performed successfully, leading to the formation of the radioactive nanocomposite **GO-[$^{124}$I]I-COSAN**, which was quickly injected in mice. PET images at different times revealed excellent *in-vivo* stability of the developed nanomaterial. No activity in thyroid and stomach was observed even at long times, proving that iodide did not detach from the material. **GO-[$^{124}$I]I-COSAN** presented a favourable biodistribution profile, being mainly accumulated in the liver and slightly in the lung, with long residence time on blood and progressive elimination via gastrointestinal tract. Noteworthy, the high boron content of this material paves the way towards theranostics, since benefits of a traceable boron delivery for boron neutron cancer therapy (BNCT).

**Keywords:** Boron clusters, metallacarboranes, Graphene oxide, C. *elegans*, PET, boron carriers, bioimaging, HeLa cells

## Introduction

One of the more outstanding areas of development for nanomaterials is the design of efficient *in vivo* imaging probes to apply in non-invasive imaging techniques such as positron emission tomography (PET), magnetic resonance imaging (MRI) or optical imaging.[1] Nanomaterials might have physicochemical properties that facilitate the incorporation of specific contrast agents and tune their biodistribution. More remarkable is the capacity of some of these nanomaterials to integrate also a drug cargo, which allows both diagnostic and treatment of disease within the same nanoplatform, giving rise to the development of the so-called theranostic agents.[2,3]

In recent years, carbon nanomaterials such as graphene and carbon nanotubes (CNTs), have attracted the attention of the scientific community for their use in many areas, from energy to the biomedical field.[4,5,6] The interest in the synthetic carbon nanostructures lies in the broad range of morphological, structural, electronic, physical and chemical properties that they possess. Carbon nanomaterials have high biocompatibility and prolonged blood circulation times,[7] arising as attractive platforms for both detection and treatment of a wide number of diseases.[8,9]

Graphene oxide (GO) is one of the most studied derivatives of graphene, which ideally consists of a single graphene layer, functionalized with a variety of O-containing aliphatic functionalities that confer it very rich surface chemistry, but also an enhanced dispersibility in aqueous media, which facilitates its processability. In this way, its surface functionalization can be achieved by both covalent and non-covalent chemistry, which can improve solubility and biocompatibility of the systems, inducing accumulation to target cells and tissues.[10,11] GO can be functionalized with organic and inorganic compounds,[12,13] being an ideal template for the development of platforms loaded with therapeutic cargoes, that allow their use in extensive biomedical applications such as drug delivery and bioimaging, among others.[14,15]

The functionalization of GO with a wide range of materials for the rational design of drug delivery systems has recently stood out.[16] These include, but are not limited to gene and RNA therapy[17] and antitumoral drugs.[18] Particular attention has been paid to the development of materials with potential applications in cancer diagnosis and therapy. Loading anticancer agents such as chlorogenic acid onto GO allows overcoming several anticancer treatment obstacles, namely low solubility, short half-life and toxicity of the drug.[19] 3D GO-based nanocarriers modified with biocompatible polymers have recently shown to present enhanced biodegradability, drug loading (of both hydrophobic and hydrophilic cargoes), and an efficient cell membrane interaction and targeted drug delivery.[20]

Anionic metals containing boron cluster derivatives (metallacarboranes), especially the cobaltabisdicarbollide anion (or simply COSAN, $[Co(C_2B_9H_{11})_2]^-$), are compounds that have a low nucleophilic character with low charge density,[21] hydrophobicity[22,23] and exceptional chemical, thermal and photochemical stability.[24,25,26,27] The hydrophobic nature of COSAN confers high amphiphilicity to its protonated form and sodium salt. This accounts for its good solubility in both, water and organic solvents,[28] as well as for its capacity to self-assemble into micelles and monolayer vesicles in aqueous media.[29,30,31,32,33] Because of its unique properties, COSAN is able to cross the lipid bilayer membrane of cells and accumulate in different types of living cells,[34] which is confirmed by Raman[35] and fluorescence techniques.[36,37,38] Due to their potential applications, from materials science to biomedicine, COSAN derivatives have been covalently linked to different types of macromolecules,[39,27,40,41,42] Moreover, they have been grafted to the surface of nanoparticles,[43,44] $TiO_2$,[45] single-wall carbon nanotubes (SWCNTs)[46] and graphene oxide,[47] giving rise to materials with enhanced dispersibility,[48] thermal stability, electrochemical features, cellular uptake and intracellular boron release. All these properties, together with the high boron content make this anion and their derivatives ideal candidates for medical applications,[49,50] especially in boron neutron capture therapy

(BNCT).[51,52,53] BNCT is a versatile, non-invasive and promising chemoradiotherapeutic technique that targets and destroys malignant tumor cells, while restricting damage to healthy cells.[54,55,56] To date, there are few examples of boron-rich drugs for BNCT that have been tested, but with unsuccessful results due to the lack of selectivity, damaging healthy tissue. Therefore, nanotechnology opens a unique opportunity to find potentially effective boron carriers for BNCT.[57]

Previously, we have demonstrated that the chemical modification of graphene oxide (as the nanoplatform) with COSAN anions (as a boron-rich structure) results in hybrid materials with improved dispersibility in both water and organic solvents, as well as highly stable aqueous dispersions. Remarkably, the combination of this anion with GO leads to a high-boron-content material with exceptional physico-chemical and thermal properties.[47] On the other hand, it has been proven that radiolabeling of COSAN with a suitable radionuclide ($^{124}$I) enables its visualization *in vivo* by Positron Emission Tomography (PET).[58] In order to explore the biological applications of COSAN anion-graphene oxide nanocomposites, herein we have moved one step further and developed a potential theranostic agent gathering high boron loading and *in vivo* imaging capabilities. For this purpose, boron-enriched carbon-based materials tagged with the positron emitter Iodine-124 ($^{124}$I) have been designed to enable whole body imaging using PET. The efficient attachment of the monoiodinated COSAN anions (**I-COSAN**) into the GO platform was confirmed by attenuated total reflectance infrared spectrophotometry (ATR-FTIR), Raman, thermogravimetric analysis (TGA) and scanning electron microscopy/energy dispersive X-ray spectroscopy (SEM/EDX) analysis. *In vitro* cytotoxicity studies and *in vivo* tests using the animal model *C. elegans* were performed to evaluate the biocompatibility of the resulting nanocomposite. Finally, *in vivo* PET studies in wild type mice were carried out to assess *in vivo* stability, circulation time and whole body biodistribution of the developed nanoplatform.

**Results and discussion**

*1. Preparation and characterization of* ***GO-I-COSAN****.*

We have explored the synthesis of a COSAN-based material as a potential theranostic agent for biomedical imaging and boron carrier for cancer therapy. The nanocomposite (**GO-I-COSAN**) was prepared by a post-synthesis functionalization of graphene oxide (**GO**) with a monoiodinated boron-cluster (**I-COSAN**, **1**), which incorporates both a short chain with a terminal functional group that could potentially operate as an attachment point to larger platforms, and an iodine atom suitable for the incorporation of the radionuclide to enable *in vivo* imaging using PET, respectively. Compound **1** was first prepared by adding iodine crystals to a solution of [8-$C_4H_8O_2NH_3$-3,3'-Co(1,2-$C_2B_9H_{10}$)(1',2'-$C_2B_9H_{11}$)] in dichloromethane (see Experimental Part). The reaction, yielding up to 90 %, was performed at 40 ºC for 90 minutes and then left to react at room temperature overnight (**Scheme 1**). To confirm the complete substitution from B-H to B-I, the process was monitored by $^{11}$B NMR using a capillary tube filled with deuterated acetone.

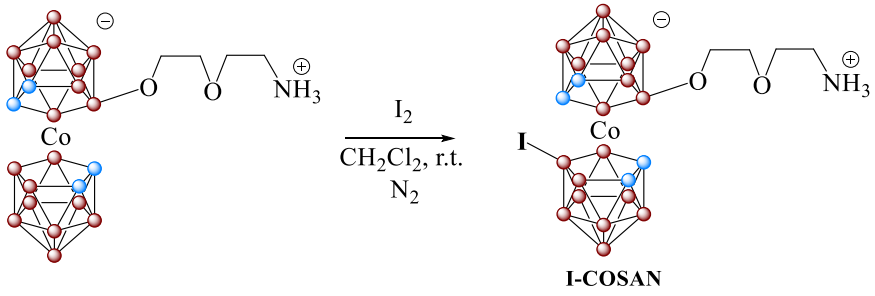


**Scheme 1**. Synthesis of iodinated COSAN derivative **I-COSAN**. Reaction conditions: [8-$C_4H_8O_2NH_3$-3,3'-Co(1,2-$C_2B_9H_{10}$)(1',2'-$C_2B_9H_{11}$)] (1.18 mmol), $I_2$ (3.16 mmol), $CH_2Cl_2$ (12 mL), 90 min reflux then overnight at r. t.

**I-COSAN**, **1**, was characterized by $^{1}$H, $^{11}$B and $^{13}$C nuclear magnetic resonance (NMR, **Figures S1-S4**),[58,59] matrix-assisted laser desorption and ionization time-of-flight mass spectrometry (MALDI-TOF MS, **Figure S5** and **Table S1**), along with Fourier-transform

infrared (FT-IR, **Figure S6**) and Raman[35,60] (**Figure S9**) spectroscopies and elemental analysis. A detailed description about the spectroscopical characterization can be found in the Electronic Supporting Information. MALDI-TOF analysis revealed the molecular peak at 552.5 m/z corresponding to M (100 %) and two main fragmentation peaks at 509.5 and 465.5, matching the loss of $CH_2CH_2NH_3$ and $CH_2CH_2OCH_2CH_2NH_3$ fragments. Elemental analysis of **I-COSAN** also confirms its chemical composition (see Experimental Part).

In parallel, **GO** was synthesized from graphite powder using a modified Hummer's method (see Experimental Part).[61] The reaction, which consists of the oxidation of graphite powder under strong oxidant/acid conditions, led to a highly exfoliated material, along with the formation of O-bearing functional groups on its surface ( *ca.* 26 wt. % of the sample, according to TGA data (*vide infra*). The structural changes induced by the oxidation treatment were confirmed by FT-IR (**Figure S7**) and Raman spectroscopy (**Figure S9**). The spectrum of **GO** showed an intense signal located at ca. 1350 $cm^{-1}$ that corresponds to the $A_{1g}$ symmetry breathing mode (D band) and confirms the presence of the oxygen-containing $sp^3$ groups disrupting the well ordered $sp^2$ conjugated system of the graphene layers, which vibration is associated to the G band, located at 1590 $cm^{-1}$.

The covalent attachment of **I-COSAN** onto **GO** was carried out *via* carboxylic acid/amine coupling, using *N,N'*-dicyclohexylcarbodiimide (DCC) and 1-hydroxybenzotriazole (HOBt) as the coupling reagents and dry THF as the solvent (**Scheme 2**).[47] The reaction mixture was stirred at 40 ºC for three days under inert atmosphere ($N_2$), and the resulting black powder was confirmed to be the desired **GO-I-COSAN** (**2**).

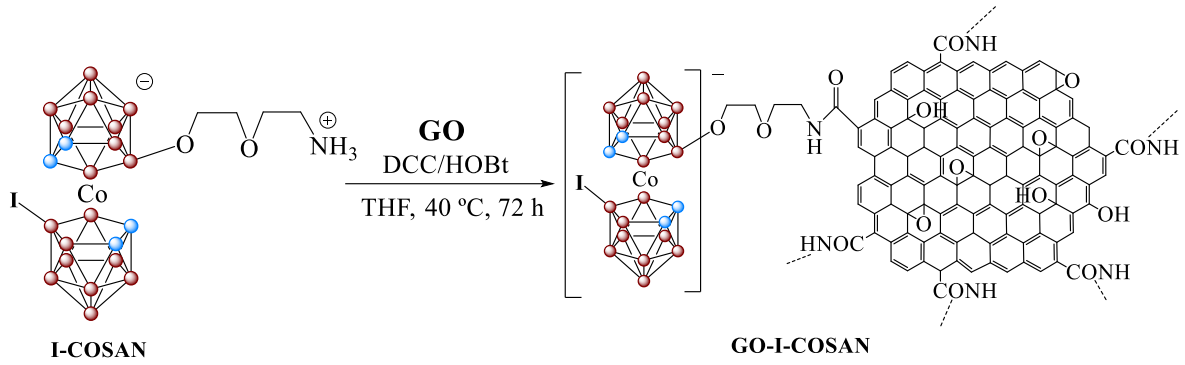


**Scheme 2**. Functionalization of GO with **I-COSAN**, yielding **GO-I-COSAN (2)**. Reaction conditions: GO (26 wt. % COOH), DCC (0.194 mmol), HOBt (0.185 mmol), THF (5 mL),1 h at r.t.; then **I-COSAN** (0.18 mmol) in THF (3 mL) for 72 h at 40 ˚C.

**GO-I-COSAN** was initially characterized by FT-IR spectroscopy (**Figure S8**). The clear band at 2543 $cm^{-1}$ attributed to υ(B-H, st) confirmed the grafting of **I-COSAN** to **GO**. Expected bands at 1720, 1571 and 1225 $cm^{-1}$, attributed to the vibration bands of the carboxylic (C=O), $sp^2$ C bonds (C=C) and hydroxyl and epoxy (C-O) groups of **GO**, respectively, were also presented. The grafting of the **I-COSAN** onto the **GO** and the subsequent formation of **GO-I-COSAN** was also observed in the Raman spectrum of the composite (**Figure S9**) with the signal corresponding to ν(B-H) (~ 2600 $cm^{-1}$).

The attachment of the boron clusters onto the **GO** surface was quantitatively determined by TGA under oxidizing atmosphere (air) (**Figure S10** and **Table S2**). The TGA curve for **GO** (**Figure S10**, dashed line) showed weight losses at ca. 220 ºC and 490 ºC, which correspond to the removal of oxygen-based functional groups attached to the **GO** surface and the total combustion of the sample, respectively. The covalent attachment of **I-COSAN** onto the **GO** surface results in a sample with less O-bearing aliphatic groups (**GO-I-COSAN**). As a consequence, a lower weight loss is observed at ca. 220 ºC for **GO-I-COSAN** (**Figure S10**, continuous line) than for **GO (Figure S10,** dotted line). As previously reported by our group,[47] the degree of functionalization can be determined from the residue after the complete combustion of the different samples. During the process all the carbon from the **GO** and the

organic part from the boron cluster compounds get oxidized. As expected, the residual mass after the complete combustion at 900 $^{o}$C is higher for **GO-I-COSAN** compared to **GO**. Unlike **GO**, annealing **GO-I-COSAN** in air led to a significant amount of residue (17.1 wt. %). This residue was considered to be mainly inorganic materials coming from oxidized boron clusters (degree of functionalization = 300 μmol·g$^{-1}$, which means ca. 58 mg B·g$^{-1}$).

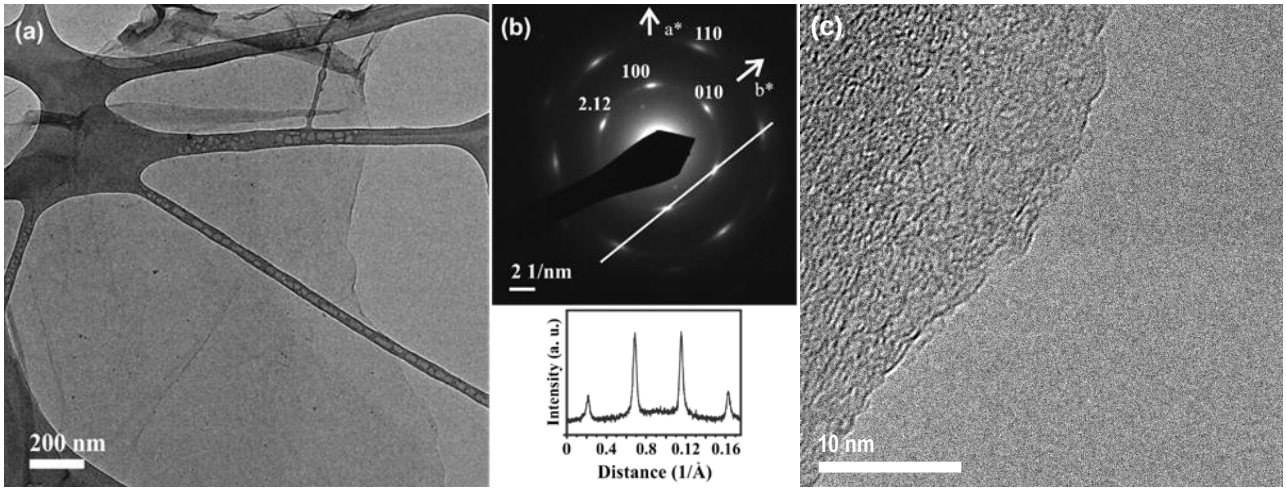


**Figure 1.** (a) TEM image of **GO-I-COSAN** and (b) SAED pattern with the corresponding line intensity profile; (c) HRTEM of **GO-I-COSAN**.

Transmission electron microscopy (TEM) was performed to evaluate the morphology of the obtained nanocomposites. TEM images of **GO-I-COSAN** (**Figure 1a**) revealed the presence of highly exfoliated graphene derivatives and the selected area electron diffraction (SAED) pattern (**Figure 1b**) confirmed the graphitic structure of the sheet ((100) and (110) planes, d spacing of 2.12 Å and 1.23 Å, respectively). Moreover, the intensity profile resulting from the diffraction spots suggested the presence of a single-layered specimen. HRTEM of **GO-I-COSAN** sheets (**Figure 1c**) confirmed the presence of exfoliated and defective few-layered **GO**, with the latter being in agreement with the performed Raman analysis where a high D-band is observed. EDX was acquired on a SEM (**Figure 2** and **Table 1**) to provide information

on the composition of the samples. The detection of cobalt signals at 0.8 and 6.9 keV, as well as those corresponding to iodine between 3.5 and 4.5 keV, confirmed the presence of the boron derivative in the material, and hence the formation of **GO-I-COSAN**. Noteworthy, equivalent atomic percentage values were obtained for cobalt and iodine in **GO-I-COSAN** (0.48 at. % for each element), confirming the purity of the precursor **I-COSAN** and the stability of the complex during attachment to **GO**. Note that the SEM image was acquired on the dry solid powder of **GO-I-COSAN**, thus leading to the observation of aggregates. It is worth noting that **GO-I-COSAN** can be readily dispersed in solvents leading to nanometer scale materials as determined by TEM observation.

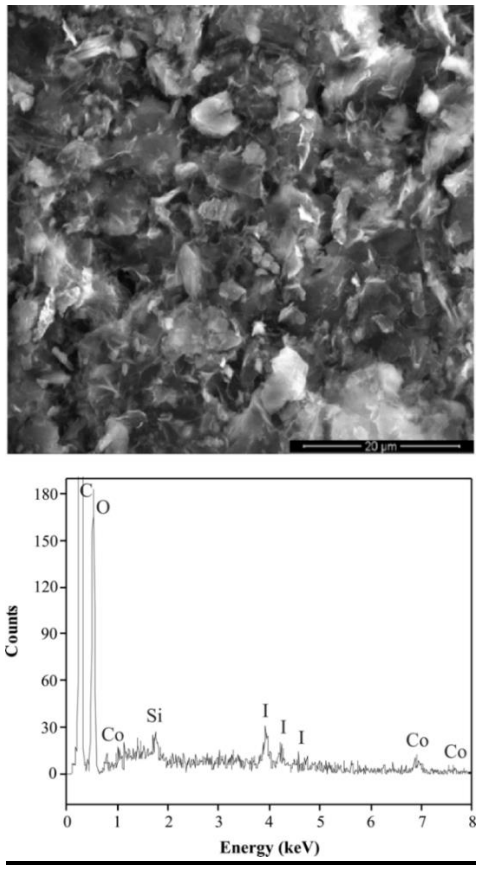


**Figure 2.** SEM image of **GO-I-COSAN** and its corresponding EDX spectrum. SEM was taken on bulk dried powder leading to the formation of aggregates.

**Table 1.** Selected EDX data showing the relative weight and atomic percentages of the different elements found in **GO-I-COSAN**.

| Element | wt. % | at. % |
|---|---|---|
| **C** | 65.49 | 71.55 |
| **O** | 14.43 | 11.84 |
| **Si** | 0.57 | 0.27 |
| **I** | 4.68 | 0.48 |
| **Co** | 2.16 | 0.48 |

*2. Cytotoxicity studies*

Before moving to radiolabeling and *in vivo* experimentation, the biocompatibility of **GO-I-COSAN** was evaluated in healthy cells. Classical colorimetric assays such as MTT or LDH can lead to false-positive results due to the interference of carbon-based nanomaterials such as graphene oxide or carbon nanotubes (CNTs), which interact with formazan crystals.[62] Therefore, a previously reported modified LDH assay, which avoids direct contact between the colorimetric indicator and the nanomaterial, was used.[63] Following this procedure, HeLa cells were incubated in 96-well plates for 24 and 48 hours in the presence of **GO-I-COSAN** at four different concentrations: 5, 12.5, 25 and 50 $\mu g \cdot mL^{-1}$. DMSO (1 % v/v) was added to culture media to improve the dispersibility of the material. Two additional samples, containing only DMSO at 1 and 10% v/v, were also included as negative and positive controls, respectively. After incubation, the media including the living cells and **GO-I-COSAN** was separated from the dead cells. The living cells were lysed with a surfactant, the media was centrifuged to remove the **GO-I-COSAN**, and the lysate cells were added to a different 96 well plate, where it was finally combined with a substrate that contained L-lactate and NAD+. This led to the formation of formazan crystals, which were analysed by UV-Vis spectrophotometry at $\lambda = 490$ nm. Hence, this "indirect" method allowed the quantification of the living cells after the

incubation, thus leading to the quantification of the dead cells by difference. The percentage of cell survival was always above 90 % (**Figure 3**), both at 24 and 48 hours of incubation and irrespective of the concentration of **GO-I-COSAN**, which confirms the low cytotoxicity for HeLa cells. HeLa is a commonly used cell line, derived from cervical cancer cells. Therefore, the viability of healthy cells could be noticeably less. As expected, high cell mortality (>80 %) after 24 hours was observed in the positive control sample, while the negative control and the control containing 1 % v/v DMSO showed similar cell viability values, thus confirming that this concentration of DMSO has no cell toxicity. TEM analysis (*vide infra*) clearly reveled that **GO-I-COSAN** was internalized by HeLa cells.

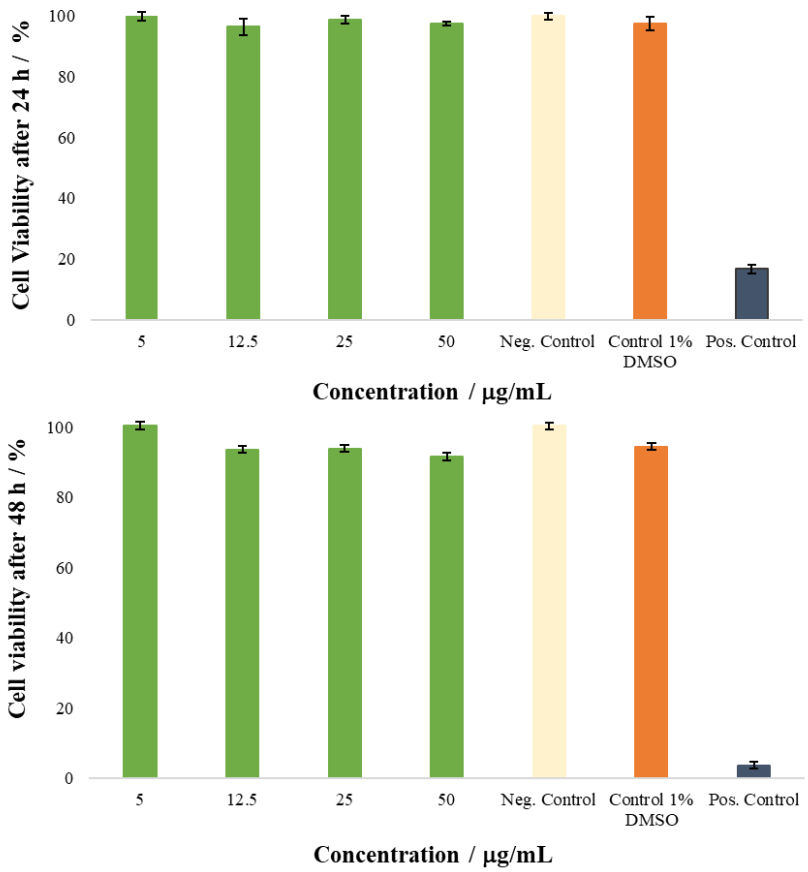


**Figure 3.** Bar graphs indicating the percentage of HeLa cell survival 24 /48 hours of treatment with 4 different concentrations of **GO-I-COSAN**, the negative control, the control with 1 vol% DMSO and the positive control (DMSO 10 vol. %), error bars mean + S.D.

Additionally, LIVE/DEAD tests were carried out for all the samples at both incubation times to confirm the results obtained in the modified LDH assay. The staining procedure was carried out using a green fluorescent calcein as marker for living cells and a red-fluorescence ethidium homodimer-1 (EthD-1) for dead cells. Images were taken using a fluorescence microscope. Calcein and EthD-1 were excited at 485 nm and 530 nm, respectively, and fluorescence emissions were acquired at 530 nm and 645 nm, respectively. **GO-I-COSAN** showed very low cytotoxicity, as the majority of cells were alive even when they were treated with the maximum concentration of the nanocomposite for 48 hours (**Figure 4**). As expected, the positive control using 10 % v/v DMSO showed a mortality rate close to 100 % after 48 hours.

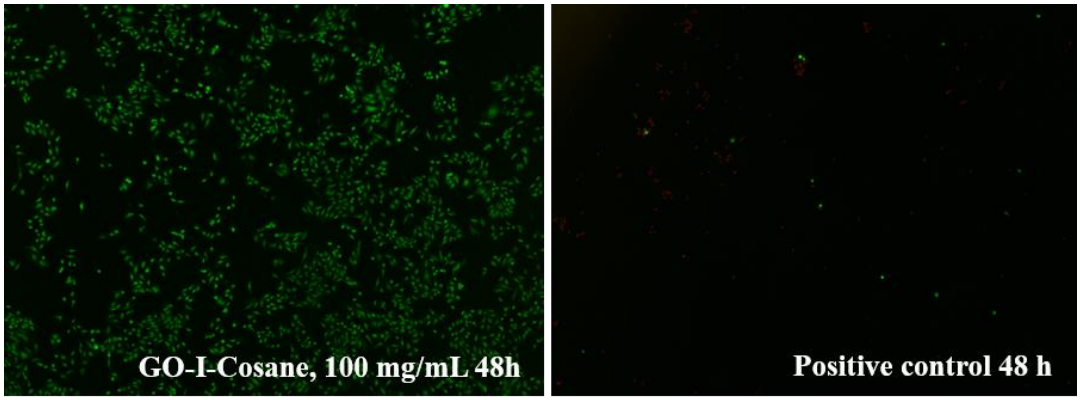


**Figure 4.** Fluorescence microscopy photographs of the LIVE/DEAD experiments of HeLa cells after being incubated for 48 h with **GO-I-COSAN**, 100 $\mu g \cdot mL^{-1}$, and DMSO 10 vol. %.

*3. Cell internalization of **GO-I-COSAN***

After confirmation of the non-cytotoxic effect of the **GO-I-COSAN** in HeLa cells, we assessed the capacity of our material to accumulate inside cells, as well as the impact on their ultrastructure. With that aim, cells were incubated with **GO-I-COSAN** for 48 h and further processed for Transmission Electron Microscopy (TEM) analysis. TEM images clearly revealed the internalization of the material by the cells, since **GO-I-COSAN** aggregates can

be observed in the cytoplasm (**Figure 5**), while no material was observed in the cell nucleus under imaging conditions used. These results are in good agreement with previously reported data using different COSAN-based fluorescent conjugates. These previous studies, performed with fluorescence confocal microscopy, showed that these dyes are able to cross the cell membrane and accumulate in the cytoplasm, thus producing an excellent cytoplasm staining.[37,38] This effect could be attributed to the COSAN strong interaction with proteins,[64,65] which results in accumulation in the cell cytosol and prevents its diffusion through the nuclear envelope's membranes and/or its passage through the nuclear pores.[34] Of note, neither the size nor the morphology of the cells was affected by the presence of **GO-I-COSAN** in the cytosol. This observation suggests that the quantity of material accumulated inside cells does not alter the structure of the cell that may lead to cell inactivity, death and formation of tissue scars. Altogether, our results confirmed that **GO-I-COSAN** has been internalized by cells without causing any cytotoxicity.

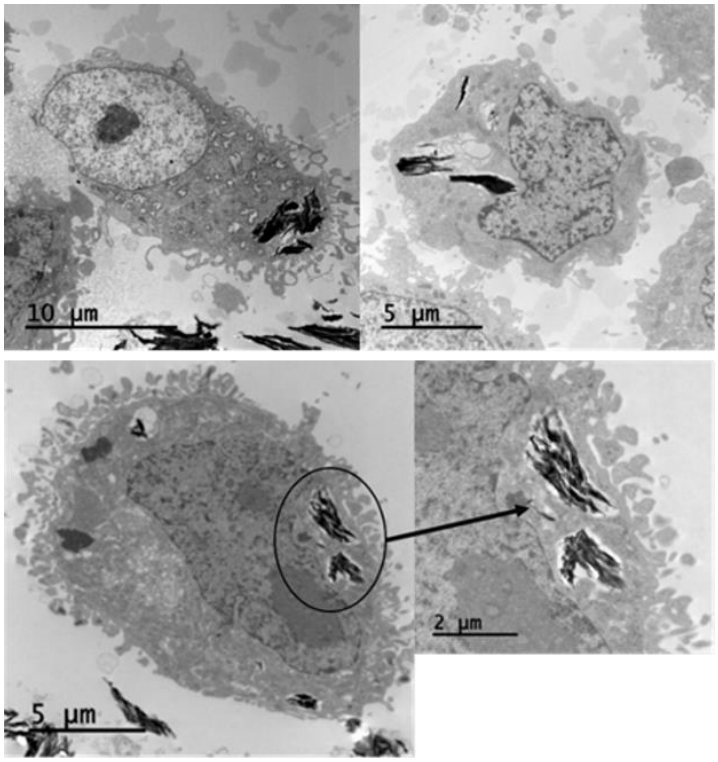

**Figure 5.** TEM images of accumulation of **GO-I-COSAN** inside HeLa cells after 48 h of incubation with solutions of 0.05 M of **GO-I-COSAN**.

*4. In vivo cytotoxicity tests with* C. elegans

After performing the *in vitro* testing of **GO-I-COSAN**, and confirming its lack of toxicity towards mammalian cells, we evaluated its toxicity *in vivo* in the small invertebrate *Caenorhabditis elegans* (*C. elegans)*, which can provide further evidence of the toxicity behaviour of the nanomaterial before moving to PET imaging experiments in rodents. *C. elegans* is a free-living nematode that has been used by scientists for decades as a model for *in vivo* experimentation due to its simplicity, easiness to grow in large populations and transparency, which makes it ideal for studying the biointeraction of opaque materials, such as **GO-I-COSAN**. Therefore, a series of assays were carried out in this living organism to determine the toxicity of the nanomaterial after 24 h of exposure time. The precursor **I-COSAN** was also tested to compare potential differences between the toxicity of the boron derivative before and after attachment to **GO**. Firstly, we confirmed that worms were able to uptake both materials (**I-COSAN** and **GO-I-COSAN**) before evaluating their toxicity. Black boluses moving along worms' intestine were localized for **GO-ICOSAN**-exposed worms (**Figure 6** and **Video S1 in the SI**), indicating that nanomaterials are ingested by *C. elegans* without any visual damage. Conversely, **I-COSAN** was not physically observed inside worms, probably due to its light color, although it is highly likely that they were also internalized, considering that the worms were able to uptake a far larger structure such as the nanocomposite.

The toxicity of **GO-I-COSAN** was studied by the survival rate and growth of the nematodes. The survival rate of the worms after incubation with both compounds was equivalent to the control group and near 100 % (**Figure 6**). The length of worms slightly decreased (ca. 4 %) in the presence of the nanomaterial. These results are in good agreement with *in vitro* tests (see

above), and further confirm the lack of toxicity of the nanomaterial, thus paving the way for further evaluation in rodents using *in vivo* imaging.

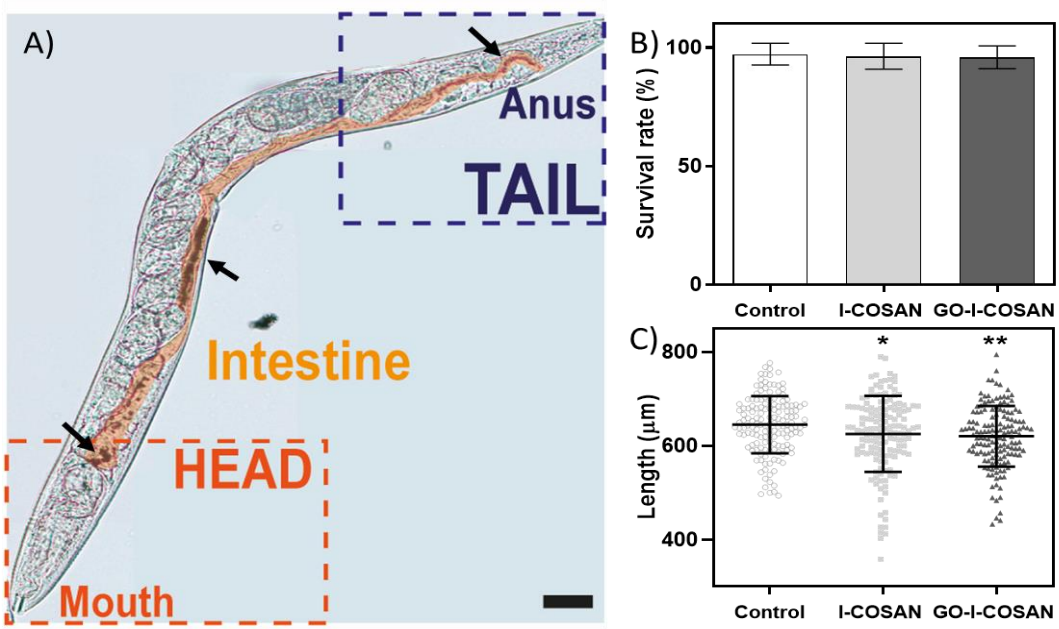


**Figure 6.** *In vivo* evaluation of **I-COSAN** and **GO-I-COSAN** in *C. elegans* model. A) Bright-field microscope image of *C. elegans* after 24 hours of incubation with **GO-I-COSAN** at the intestinal region (arrows). Labels and colored intestine of *C. elegans* are added for clarity. Scale bar= 30 µm. B) Survival rate (N=3, n=450); C) Length of worms (N=3, n=150) was evaluated after 24 h of nanomaterials exposure. * p<.05 **p<.001.

*5. Radiolabeling and PET imaging*

PET imaging is a fully translational molecular imaging technique that allows the visualization of positron emitter-labeled entities after administration into living organisms. Its high sensitivity and minimal invasive character turn this modality into the option of choice to assess whole body biodistribution of new chemical entities.

Nanomaterials are expected to have long residence times in the organism. Hence, and in order to get long-term quantitative information, iodine-124 ($^{124}I$, $t_{1/2}$ = 4.2 days) was selected. Taking advantage of the presence of an iodine atom on the COSAN structure, radiolabeling was

approached by isotopic exchange, following a previously reported method.[58] However, the setup of the experimental conditions was performed with the more affordable and available $^{131}$I radionuclide ($t_{1/2}$= 8 days). In brief, **I-COSAN** was reacted with Na[$^{131}$I]I (50 µL, 74 MBq, 0.1 M aqueous NaOH solution) in the presence of Herrmann's catalyst (0.1 mg solution in toluene) for 8 minutes at 100 ºC to achieve [**$^{131}$I]I-COSAN** in 75 % incorporation ratios (**Scheme 3**). Longer reaction times led to the formation of unidentified side products, as determined by radio-high performance liquid chromatography (radio-HPLC), resulting in lower radiochemical yields. Hence, the above-mentioned conditions were used in subsequent experiments. Quality control of the purified compound confirmed a non decay-corrected radiochemical yield of 70% with respect to Na[$^{131}$I]I and close-to-quantitative recovery of I-COSAN.

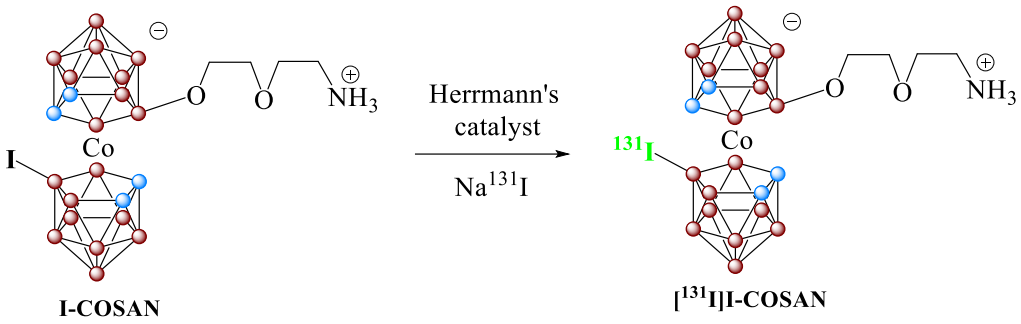


**Scheme 3**. Radiolabeling reaction of **I-COSAN** with Na[$^{131}$I]I to obtain **[$^{131}$I]I-COSAN**. Reaction conditions: Na[$^{131}$I]I (50 µL, 74 MBq), acetonitrile (100 µL), Herrmann's catalyst (0.101 µmol) in toluene (100 µL) at 100 °C for 10 min.

After successful radiosynthesis of [**$^{131}$I]I-COSAN,** the coupling reaction with **GO** was tackled. The purified [**$^{131}$I]I-COSAN** (containing ca. 1 mg of I-COSAN and an amount of radioactivity of ca. 52 MBq) was dissolved in DMF (1 mL) and reacted with **GO** (1 mg) in the presence of DCC/HOBt mixture (1+1 mg) at 40 ºC for 72 hours, resulting in the formation of **GO-[$^{131}$I]I-COSAN** as a black solid with a radiochemical yield (decay corrected) of ca. 11 % with respect

to [$^{131}$**I]I-COSAN** (non-decay corrected yield = 8.5%). In spite of the low yield, the final amount of radioactivity (ca. 4.4 MBq) was sufficient for eventual *in vivo* experiments, and hence the experimental conditions were not further optimized. Hence, the conditions were applied to the preparation of **GO-[$^{124}$I]I-COSAN** (**Scheme 4**). With that aim, **[$^{124}$I]I-COSAN** was first prepared by starting from **Na[$^{124}$I]I** (74 MBq). The purified compound (containing ca. 1 mg of **I-COSAN**) was reacted with **GO** (1 mg) to yield **GO-[$^{124}$I]I-COSAN** with a non-decay corrected radiochemical yield of 6.5 % with respect to [$^{124}$**I]I-COSAN**. The final amount of radioactivity was 3.4 MBq.

Considering that **I-COSAN** and **[$^{124}$I]I-COSAN** equally reacts towards **GO**, and that the decay corrected yield of the coupling reaction is 11%, the amount of **I-COSAN** in the final nanocomposite was 0.11 mg per mg of **GO**, which resulted in a boron content of 47 µg per mg of **GO** (4.5% load of **I-COSAN** in the final nanomaterial; specific activity: 3.3 MBq/mg).

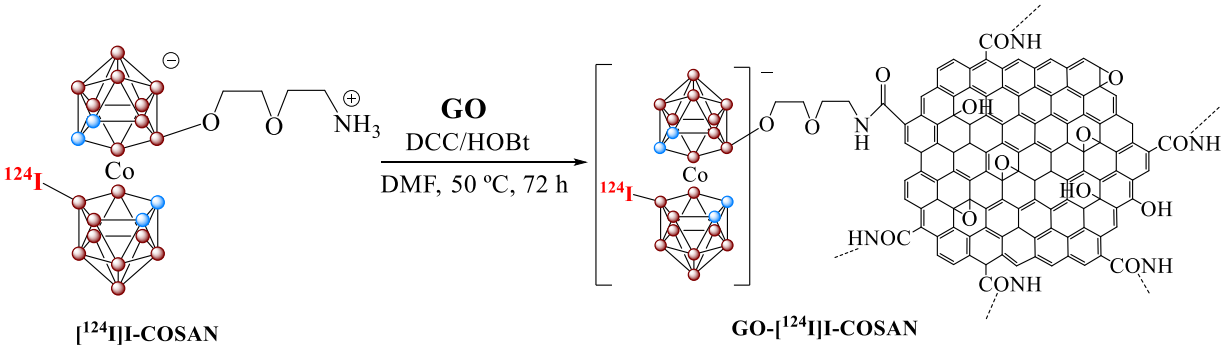


**Scheme 4**. Functionalization of **GO** with **[$^{124}$I]I-COSAN** leading to radioactive species **GO-[$^{124}$I-COSAN]**. Reaction conditions:**[$^{124}$I]I-COSAN** (ca. 1.6 MBq), DMF (1 mL), **GO** (1 mg), DCC (1 mg) and HOBt (1 mg) at 50 °C for 3 days.

The resulting **GO-[$^{124}$I]I-COSAN** was dispersed in physiologic saline solution containing ethanol (10 % v/v) and whole body PET imaging studies were carried out immediately after intravenous administration into mice. The administered dose was 1.5-2.0 MBq, which means that the mass amount administered to animals was in the range 0.45-0.60 mg (20.2-27.0 µg of

boron). Static images were also obtained at t= 4, 24 and 48 hours after administration. Visual inspection of the PET images (**Figure 7**) shows major accumulation of radioactivity in the liver and the lungs at short times after administration. This result was expected, as nanomaterials in this size range are, to some extent, accumulated in the organs of the mononuclear phagocytic system (MPS). The presence of radioactivity can also be detected in the heart, suggesting the presence of **GO-[$^{124}$I]I-COSAN** in the blood pool. At longer time points, an intense signal was still visualized in the liver, although progressive accumulation in the gastrointestinal tract was detected, with elimination via feces at t = 48 hours, as clearly visualized in coronal and sagittal views. Noteworthy, the images at late time points did not show accumulation of the radioactivity in the stomach. This result, along with the lack of accumulation in the thyroid gland, strongly indicated the radiochemical stability of **GO-[$^{124}$I]I-COSAN** *in vivo*, as no free radioiodide was released. Likewise, if the **[$^{124}$I]I-COSAN** remains attached to the **GO** cannot be confirmed; however, the long residence time in the liver suggested stability of the nanocomposite, although further experiments to investigate the co-localization of both components of the nanocomposite might be required. This could be achieved, for example, by using a dual labeling approach as previously described.[66]

In order to get quantitative data, volumes of interest (VOIs) were manually drawn in organs easily identified on the CT images, namely the brain, the lungs, the heart, the liver, the kidneys and the bladder, and the concentration of radioactivity was determined as percentage of injected dose per cm$^3$ (% ID/cm$^3$) (**Figure 7**). Quantitative data confirmed high accumulation in the liver at early times, with average values of 24.7 and 23.2 % ID/cm$^3$ at t=0 and 4 hours after administration. Significant accumulation was also observed in the lungs (9.9 and 13.6 %ID/cm$^3$ at t=0 and 4 hours, respectively) and the kidneys (6.4 and 7.9%ID/cm$^3$ at t=0 and 4 hours, respectively). Interestingly, no accumulation was observed in the bladder over the whole duration of the study, confirming thus the lack of elimination via urine. The presence of

radioactivity in the heart can be considered as a surrogate of the presence of radioactivity in blood. The high values at t = 24- and 48-hours post-administration (8.0 and 6.3 % ID/cm$^3$, respectively) are particularly interesting, as they demonstrate the long circulation time of a fraction of the radioactivity, which is essential to achieve tumor accumulation via EPR effect. Quantification of the amount of radioactivity in the gastrointestinal tract and the stomach could not be carried out, due to the difficulties in delineating volumes of interest in these organs on the CT images. Altogether, these results showed favourable biodistribution profiles with long residence time on blood and progressive elimination via gastrointestinal tract, suggesting potential application of our nanosystems as theranostic agents for BNCT.

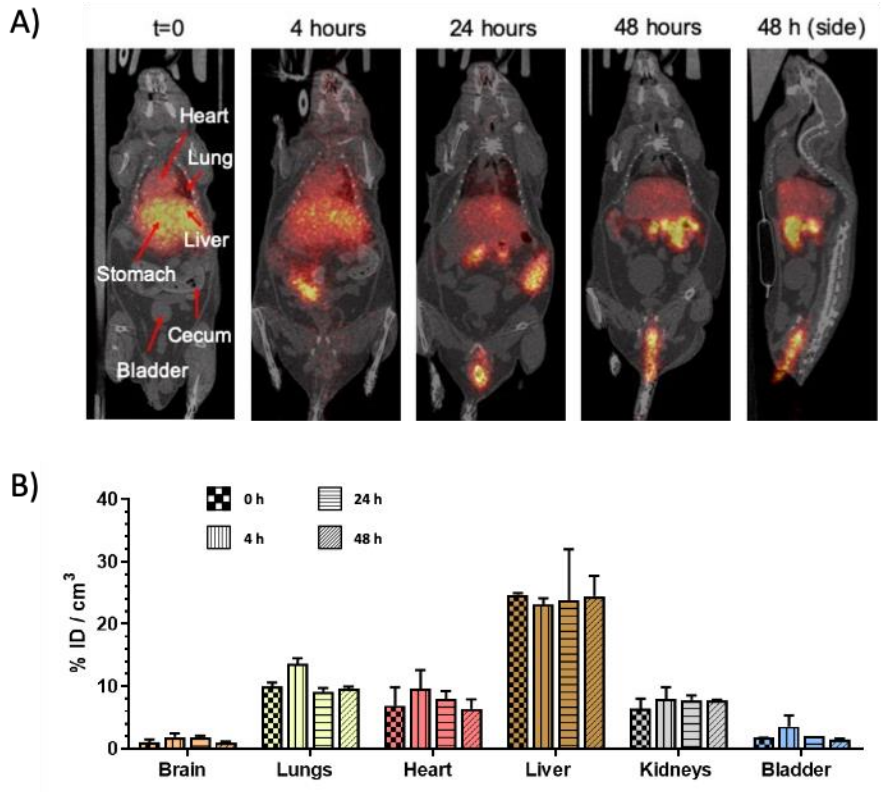


**Figure 7.** A) PET images (maximum intensity projections, coronal views) obtained at different time points after intravenous administration of **GO-[$^{124}$I]I-COSAN** in mice. PET images have been co-registered with representative computed tomography (CT) slices of the same animal for anatomical localization of the radioactive signal. On the right, a sagittal view of the animal at t=48h after administration is shown; B) concentration of radioactivity in different organs at different time points after intravenous administration of **GO-[$^{124}$I]I-COSAN** in mice, as determined from PET images. Values are expressed as mean ± standard deviation, n = 2.

## Conclusions

A carbon-based material has been prepared by the efficient covalent functionalization of graphene oxide (**GO**) with a monoiodinated cobaltabisdicarbollide derivative **I-COSAN**. The **GO-I-COSAN** nanocomposite did not show cytotoxicity *in vitro* for HeLa cells, with a cell viability greater than 90 %. TEM analyses confirmed the internalization of the material by cells, which was mainly accumulated in the cytoplasm, without causing changes neither in the size nor in the morphology of cells. Furthermore, **GO-I-COSAN** was ingested by *C. elegans* resulting in a survival rate of around 100 %, revealing the absence of toxicity *in vivo* for the worms and supporting the results observed in the *in-vitro* studies. Radiolabeling of the material with the positron emitter $^{124}$I was achieved via isotopic exchange of the **I-COSAN** to obtain **[$^{124}$I]I-COSAN** followed by its grafting onto **GO**. Biodistribution studies by PET indicated accumulation of the material in the liver at early time, as well as accumulations in lungs and kindness. Notably, a favourable biodistribution profile, with long residence time on blood and progressive elimination via gastrointestinal tract, suggested the potential use of this nanomaterial as a theranostic agent for *in vivo* bioimaging and boron carriers for BNCT.

**Experimental section**

**Characterization.** The $^{1}H$ NMR (400 MHz), $^{11}B$ and $^{11}B$ $\{^{1}H\}$ (128.38 MHz) and $^{13}C$ $\{^{1}H\}$ NMR (100 MHz) spectra were acquired on a Bruker Avance-III spectrometer. All NMR spectra were recorded in $CD_3COCD_3$ (purchased from Eurisotop) solutions at 22 ºC. $^{1}H$ and $^{13}C$ $\{^{1}H\}$ NMR spectra were referenced to TMS, whilst $^{11}B$ spectra were referenced to external $BF_3 \cdot OEt_2$. Chemical shifts are reported in units of parts per million downfield from the reference and all coupling constants are reported in Hz.

FT-IR spectra were recorded using a Perkin Elmer Spectrum One spectrometer. Samples were prepared by using a ZnSe pellet (2 mm thickness) by drop-drying sample dispersions on 2-propanol onto a preheated hot plate at 80 ºC.

MALDI-TOF Mass Spectra were collected in the negative mode using a Bruker Biflex instrument ($N_2$ laser; $\lambda_{exc}$ 337 nm, pulses of 0.5 ns), with an ion source of 20000 kV (Uis1) and 17500 kV (Uis2). Due to the nature of the compounds, a matrix was not necessary. CHNS Elemental analysis was performed using a MX5 Mettler Toledo microbalance and a Thermo Scientific Flash 2000 analyzer.

TGA analyses were performed under flowing air at a heating rate of 10 °C $min^{-1}$ up to 900 °C using a Jupiter (Netzsch Instrument, Germany) thermogravimeter analyzer.

SEM images and EDX analyses were performed using on a QUANTA FEI 200 FEG-ESEM microscope. TEM images and SAED patterns were obtained using a JEOL 1210 microscope, operated at 120 kV. HRTEM images were obtained using a Jeol JEM 2011 cryo-electron microscope operated at 200 kV, recorded on a Gatan Ultrascan US1000 CCD camera and analysed with a Digital Micrograph 1.8

**Materials**. All reactions were performed under an atmosphere of dinitrogen employing standard Schlenk techniques. [8-$C_4H_8O_2NH_3$-3,3'-Co(1,2-$C_2B_9H_{10}$)(1',2'-$C_2B_9H_{11}$)] were obtained as described in the literature.[47,59,67] Reagent grade iodine was purchased from Aldrich and used as received. Solvents and all other reagents were purchased from Aldrich and used as received. Reactions were monitored by thin layer chromatography (TLC), using an appropriate solvent system. Silica coated aluminium TLC plates used were purchased from Merck (Kieselgel 60 F-254). GO was synthesized using Graphite powder (< 20 μm), purchased from Sigma-Aldrich.

**Synthesis of Graphene oxide (GO).** Graphene oxide (**GO**) was synthesized by a modified Hummer's method.[61] Keeping the temperature down to 0 °C, graphite powder (2.5 g), concentrated $H_2SO_4$ (57.5 mL) and $NaNO_3$ (1.25 g) were mixed together. After 30 min (at 0 °C ), 7.5 g of $KMnO_4$ were added slowly, maintaining the system below 20 °C. The mixture was stirred and warmed to 35 °C during 30 min, the reaction was cooled to room temperature and then 115 mL of water were added, carefully. The system was kept under reflux (98 °C) for 2 h and after cooling down, additional water (500 mL) and 2.5 mL of 30 % $H_2O_2$ solution were finally added. The sample was purified by consecutive centrifugation cycles (20000 rpm), washing with distilled water until neutral pH was reached. The recovered black powder was dried at 60 °C overnight and subsequently ground using an agate mortar and pestle.

**Synthesis of [8-$C_4H_8O_2NH_3$-3,3'-Co(1,2-$C_2B_9H_{10}$)(8'-I-1',2'-$C_2B_9H_{11}$)] (1 or I-COSAN).** In a oven-dried 25 mL round-bottomed flask, freshly synthesized [8-$C_4H_8O_2NH_3$-3,3'-Co(1,2-$C_2B_9H_{10}$)(1',2'-$C_2B_9H_{11}$)] (505 mg, 1.18 mmol) and iodine crystals (800 mg, 3.16 mmol) were dissolved in $CH_2Cl_2$ (12 mL). The reaction mixture was heated under reflux for 90 minutes and then stirred overnight at room temperature. Afterwards, the solvent was evaporated under

vacuum and the red residue was extracted three times with 25 mL of $Et_2O$, washed once with 25 mL of a saturated aqueous solution of $NaHSO_3$ and finally once with 25 mL of water. The organic phase was dried with $MgSO_4$, prior to the removal of the solvent under vacuum until a dark orange oil was obtained. This was further purified by silica gel column chromatography using in first place a 90 % ethyl acetate – 10 % hexane mixture until a yellowish product was eluted, then pure methanol was added to elute **1** as a pure orange solid. Yield: 590 mg, 90 %. $^1$H NMR ($CD_3COCD_3$, TMS), δ (ppm): 7.82 (br s, 3H, $N^+H_3$), 4.43 (br s, 2H, $C_c$-*H*), 4.24 (br s, 2H, $C_c$-*H*), 3.87 (t, 2H, $^3$J(H-H)= 6 Hz, $CH_2N^+H_3$), 3.57 (m, 6H, $CH_2O$), 3.14 (br s, 2H, B-H), 3.00 (br s, 2H, B-H), 2.86 (br s, 2H, B-H), 2.40 (br s, 2H, B-H), 1.70 (br s, 4H, B-H).$^{11}$B NMR ($CD_3COCD_3$, $BF_3{\cdot}Et_2O$), δ (ppm): 21.63 (s, 1B, B-O), -0.49 (d, 2B, $^1$J(B-H)=118 Hz), -4.64 (d, 2B, $^1$J(B-H)=131 Hz), -5.61 (d, 4B, $^1$J(B-H)=191 Hz), -7.23 (d, 3B, $^1$J(B-H)=139 Hz), -17.94 (d, 2B, $^1$J(B-H)=159 Hz), -19.91 (d, 2B, $^1$J(B-H)=160 Hz), -23.46 (d, 1B, $^1$J(B-H)=151 Hz), -27.29 (d, 1B, $^1$J(B-H)=171 Hz). $^{13}$C {$^1$H} NMR ($CD_3COCD_3$, TMS), δ (ppm): 71.49 ($C_{alkyl}$), 68.28 ($C_{alkyl}$), 67.48 ($C_{alkyl}$), 56.37 ($C_c$-H), 54.45 ($C_c$-H). ATR ($cm^{-1}$): 3221 (w, N-H st), 3038 (w, C-$H_{cluster}$ st), 2918 (w, C-$H_{alkyl}$ st), 2868 (w, C-$H_{alkyl}$ st), 2540 (s, B-H st), 1598 (w, H-N-H δ), 1091 (s, C-O st). MALDI-TOF-MS (m/z): 575.3 ([M+$Na^+$], 4.0 %), 552.5 ([$M^+$], 100 %), 509.5 ([$M^+$-$CH_2CH_2NH_3$], 33.0 %), 465.5 ([$M^+$-$CH_2CH_2OCH_2CH_2NH_3$], 31.4 %). Anal. Calcd. for [8-$C_4H_8O_2NH_3$-3,3'-Co(1,2-$C_2B_9H_{10}$)( 8'-I-1',2'-$C_2B_9H_{11}$)] (%): C, 17.32; H, 5.77; N, 2.52. Found: C, 18.85; H, 5.89; N, 2.26 (+1 molecule of $CH_3OH$).

**Synthesis of GO-[8-$C_4H_8O_2NH_3$-3,3'-Co(1,2-$C_2B_9H_{10}$)(8'-I-1',2'-$C_2B_9H_{11}$)] (2 or GO-I-COSAN). GO** (28 mg, 26 wt. % COOH) was dried for 2 h at 100 ˚C under vacuum. Then, DCC (40 mg, 0.194 mmol), HOBt (25 mg, 0.185 mmol) and dry THF (5 mL) were added and the heterogeneous mixture was stirred for 1 h at room temperature, followed by addition of a

solution of **1** (100 mg, 0.180 mmol) in THF (3 mL). The reaction was stirred for 72 h at 40 ˚C, the solvent was removed under vacuum and the residue was washed with methanol, filtered through a 0.2 μm polycarbonate membrane (Millipore) and washed again with MeOH. The sample was then dried to obtain **2** as a black solid. FT-IR (ZnSe pellet, $cm^{-1}$): 2543 (w, B-H st), 1720 (m, C-O st), 1571 (m, C-O st), 1225 (m, C-O st).

**Cytotoxicity Assays**

Four different solid samples of **GO-I-COSAN** were prepared, one for each concentration (10, 25, 50 and 100 $\mu g \cdot mL^{-1}$, with the intention of diluting them in half during the procedure). These samples were sterilized by overnight UV germicidal irradiation and diluted in DMSO (1% final concentration) and, after 1 minute of sonication, each sample was diluted in culture media (MEM-alpha supplemented with 10% Fetal bovine serum and Penicilin-Streptomicin-Fungizone solution (GIBCO)). Samples were sonicated for 1 hour.

HeLa cells (ATCC CCL-2) were used to perform the biological assays. Cells were maintained in MEM-alpha supplemented with 10% Fetal bovine serum and 4mM L-Glutamine at 37ºC and an atmosphere of 5% $CO_2$.

Cytotoxicity of **GO-I-COSAN** was tested at 24h and 48h. HeLa cells were seeded in 96-well plates (3500 cells/well for 24h and 1800 cells/well for 48h) with 100μl of culture media per well, and kept for 24 hours in standard culture conditions to allow cell adhesion. Then 100 μl of each tested concentration of **GO-I-COSAN** were added to the corresponding well and incubated for 24 or 48 hours. The effect of **GO-I-COSAN** in cell viability was assessed using a modified LDH assay (CytoTox 96 non-radioactive cytotoxicity assay, Promega) described in Ali Boucetta *et al*.[63] Cell viability was also analyzed using the live/dead viability/cytotoxicity kit (Thermo Fisher) based on the cellular esterase activity and membrane integrity. HeLa cells were seeded in a 24-well plate (10700 cells/well for 24h and 20700 cells/well for 48h). Live

cells were stained in green and microphotographs were taken in a Nikon inverted fluorescence microscope.

***C. elegans in vivo* evaluation.** *Caenorhabditis elegans (C. elegans)* Bristol strain N2 and *Escherichia coli* OP50 were obtained from the Caenorhabditis Genetic Center (CGC). Nematodes were maintained using standard procedures at 20 ºC,[68] and exposure was performed following previous protocols.[69] Synchronized L4 well-fed worms with OP50 were rinsed with S-basal buffer and washed three times to remove OP50. Worms were treated separately with S-basal buffer (control), 25 μg·mL$^{-1}$ of **I-COSAN,** and 25 μg·mL$^{-1}$ of **GO-I-COSAN** in a final volume of 100 μl for 24 h. The survival assay was performed, tapping the plate and counting as alive worms those that moved.[69] Each well contained 9 ± 3 adult worms (N=3, n=450). For the length experiment, control and exposed young adult worms were cleaned three times and fixed with paraformaldehyde (PFA 1 %) after the exposure, and they were mounted in a microscope slide to evaluate the effect in growth. The length of 50 worms per condition (N=3, n=150) was measured using ImageJ-Fiji Software. Images were taken with a microscope Olympus RXSITRF 52787, MAB INDUSTRIAL. Both assays, survival rate and growth effects were performed in triplicate. For statistical analysis, One-way ANOVA with Turkey post-correction was performed using GraphPad Prism version 5.

**TEM of HeLa cells.** To prepare the samples necessary for this assay, HeLa cells (CCL-2) p.X+17 from American type culture collections were used. The medium culture for cell seeding was MEM-alpha supplemented with 10 % Fetal bovine serum (1), whereas the medium culture for assay (2) included a solution of antibiotics Penicilin-Streptomicin-Fungizone to prevent bacterial contamination. On the first day, three 75 cm$^2$ T-flasks with HeLa cells with 15 mL MEM-alpha medium (1) were seeded whilst **GO-I-COSAN** (0.5 mg, duplicate) was sterilized

in a laminar airflow hood with a UV light fluorescent lamp overnight. After, 1 vol % DMSO (100 μL) were added to the **GO-I-COSAN**, which were subsequently vortexed for a few seconds and sonicated for 1 minute. The solutions were transferred to a sterilized test tube that contained 10 mL of fresh medium culture (2) and sonicated for one hour. Then, the solution medium (1) was removed from the cell culture and the **GO-I-COSAN** solutions in assay medium (2) were added to the cells (in duplicate). A 10 mL control solution was also prepared in the same conditions. The three samples -two **GO-I-COSAN** duplicates and the control- were incubated for 48 hours at 37 ºC in the incubator at 5 % $CO_2$. After, the cells were washed twice with PBS and trypsinized. The resulting pellets were transferred to a test tube and centrifuged for 6 minutes at 1500 rpm in PBS. The cells were then fixed with 4% formaldehyde in PBS for 15 min at room temperature. Els pellets were recovered with the fixer solution and transferred to the Eppendorf, which were previously washed with PBS (2 mL), and kept at 4 ºC. The samples were then dehydrated in graded ethanol series and propylene oxide, and embedded into Durcupan (Fluka AG, Switzerland). Ultrathin (60 nm) sections were cut by Power-Tome MT-XL (RMC/Sorvall, Tucson, USA) ultramicrotome, placed on copper grids covered with epon and spur resins, and contrasted by lead citrate.[70] The sections were examined with a Jeol 1400 electron microscope (Jeol Ltd.) working at 80 kV and equipped with a GatanOrius SC200 CCD camera (Gatan Inc.). For each sample and technique, representative images of different fields were captured at high magnifications (from 100,000x to 600,000x).

**Radiochemistry.** Radiolabeling reactions on compound **I-COSAN** was performed following a previously reported method,[58] with minor modifications. The assays for the set up of the experimental conditions were carried out using $^{131}I$, while $^{124}I$ was used for *in vivo* experiments. Na[$^{131}I$]I (solution in 0.1 M aqueous NaOH) and Na[$^{124}I$]I (solution in 0.02 M aqueous NaOH) were obtained from Perkin Elmer and used without further purification. All solvents were

HPLC grade and were degassed for 10 minutes before use. The manipulation of radioactive materials was performed in lead-shielded cabinets (75 mm of lead) and all procedures were performed according to the current regulation on radioprotection and internal protocols.

**Synthesis of [8-$C_4H_8O_2NH_3$-3,3'-Co(1,2-$C_2B_9H_{10}$)(8'-[$^{131}$I]-1',2'-$C_2B_9H_{11}$)] (3 or [$^{131}$I]I-COSAN).** Acetonitrile (100 µL) was added to Na[$^{131}$I]I (50 µL, 74 MBq) and the resulting solution was introduced in a 2.5 mL conic vial. The solvent was evaporated to dryness (100 °C, 10 min, constant helium flow at 20 mL·min$^{-1}$) and the precursor (compound **I-COSAN**; 1 mg) dissolved in acetonitrile (100 µL) was added together with *trans-bis*(acetate)*bis*[o-(di-o-tolylphosphino)benzyl] dipalladium (II) (Herrmann's catalyst, HC, 0.1 mg, 0.101 µmol) dissolved in toluene (100 µL). The reaction mixture was heated at 100 °C for different times (5-15 min), the solvent was removed under a constant helium flow and the resulting solid was dissolved in 0.5 mL acetonitrile and 30 mL of ultrapure water. The crude solution was passed through a C-18 cartridge (Sep-Pak® Light, Waters) and washed with ultrapure water (2 × 5 mL) to remove free iodine. The final product (**[$^{131}$I]I-COSAN**) was eluted from the cartridge with ethanol (500 µL). The solvent was finally evaporated to dryness. Quality control was performed by radio-HPLC after diluting the solid residue with mobile phase. Analytical conditions were: Stationary phase: Mediterranea Sea18 column (4.6 x150 mm, 5 µm particle size, Teknokroma, Spain); mobile phase A: 0.1 M ammonium formate (AMF) buffer pH= 3.9; B: acetonitrile; flow rate = 1mL·min$^{-1}$; gradient: 0 min: 60 % A- 40 % B; 2 min: 60 % A- 40 % B; 6 min: 20 % A- 80 % B; 14 min: 0 % A- 100 % B; 16 min: 0 % A- 100 % B; 18 min: 60 % A- 40 % B; 20 min: 60% A- 40% B (retention time: 10.5 min). The concentration of **I-COSAN** in the final solution, to evaluate recovery of the compound, was determined by HPLC using the same analytical method, and using a calibration curve generated from reference standard solutions.

**Synthesis of [8-$C_4H_8O_2NH_3$-3,3'-Co(1,2-$C_2B_9H_{10}$)(8'-[$^{124}$I]I-1',2'-$C_2B_9H_{11}$)] (4 or [$^{124}$I]I-COSAN).** The preparation of this compound was carried out following the procedure described above, using Na[$^{124}$I]I (solution in 0.02 M aqueous NaOH). Reaction time was set to 8 minutes, as this provided the highest yield while avoiding the formation of by-products.

**Synthesis of GO-[8-$C_4H_8O_2NH_3$-3,3'-Co(1,2-$C_2B_9H_{10}$)( 8'-$^{131}$I-1',2'-$C_2B_9H_{11}$)] (5 or GO-[$^{131}$I]I-COSAN).** The full amount of freshly prepared **[$^{131}$I]-COSAN** was dissolved in DMF (1 mL) and subsequently loaded with a syringe into a glass tube equipped with a stirring magnet and dry GO (1 mg), DCC (1 mg) and HOBt (1 mg). The mixture was allowed to react under stirring in a water bath at 50 °C for 3 days. The solid was then centrifuged, and the DMF decanted. The black solid was washed three times with ethanol and finally filtered using a centrifuge filter tube.

**Synthesis of GO-[8-$C_4H_8O_2NH_3$-3,3'-Co(1,2-$C_2B_9H_{10}$)( 8'-$^{124}$I-1',2'-$C_2B_9H_{11}$)] (6 or GO-[$^{124}$I]I-COSAN).** The preparation of **GO-[$^{124}$I]I-COSAN** was carried out following the same procedure as above, but using [$^{124}$I]I-COSAN (the whole amount obtained in the first labeling step).

**Animals.** The animals were maintained and handled in accordance with the Guidelines for Accommodation and Care of Animals (European Convention for Protection of Vertebrate Animals Used for Experimental and Other Scientific Purposes) and internal guidelines. Experimental procedures were approved by the ethical committee and local authorities. All animals were housed in ventilated cages and fed on standard diet *ad libitum*.

**Biodistribution studies.** PET-CT studies with **GO-$^{124}$I-COSAN** were carried out in healthy mice (n=2) using the gamma- and X-cube systems (Molecubes, Gent, Belgium). Anaesthesia was induced with 3 % isoflurane and maintained by 1.5 to 2 % of isoflurane in 100 % $O_2$. For intravenous administration of the radiotracer, the tail vein was catheterized with a 24-gauge catheter and the labeled NPs (ca. 1.5–2 MBq) were injected. The first image was acquired immediately after tracer administration (total duration = 10 minutes); static images were also acquired at t=4, 24 and 48 hours after administration (duration: 15 minutes per scan). After each PET session, a CT image was acquired for anatomical localization of the radioactive signal and application of attenuation correction during image reconstruction. PET images were reconstructed with OSEM3D iterative algorithm, and analysed using PMOD image analysis software (PMOD Technologies Ltd, Zürich, Switzerland). Volumes of interest (VOIs) were manually drawn in lungs, liver, heart, kidneys, brain, and bladder using CT images as anatomical reference. VOIs were then transferred to the PET images and time activity curves (decay corrected) were obtained for each organ as cps/cm$^3$. Curves were transformed into real activity (Bq/cm$^3$) curves. Injected dose normalization was finally applied to data to get time activity curves as the percentage of injected dose per cm$^3$ of tissue (% ID/cm$^3$).

## ASSOCIATED CONTENT

### Supporting Information

The Supporting Information is available free of charge on the ACS Publications website at DOI: including the spectroscopic characterization of **I-COSAN**, $^1$H NMR of **I-COSAN** (**1**) in $CD_3COCD_3$ (**Figure S1**);. $^{11}$B NMR of **I-COSAN** (**1)** in $CD_3COCD_3$ (**Figure S2**); $^{11}$B {$^1$H} NMR of **I-COSAN** (**1**) in $CD_3COCD_3$ (**Figure S3**);. $^{13}$C {$^1$H} NMR of **I-COSAN** (**1**) in

$CD_3COCD_3$ (**Figure S4**); MALDI-TOF spectrum of **I-COSAN** (**1**) (**Figure S5**); FT-IR spectrum of **I-COSAN** (**1**) (**Figure S6**); FT-IR spectrum of **GO** (**Figure S7**); FT-IR spectrum of **GO-I-COSAN (Figure S8**); Raman spectra of **GO**, **ICOSAN** and **GO-I-COSAN** (**Figure S9**); TGA of **GO-I-COSAN** (solid line) and the starting compounds **GO** (dashed line) and **I-COSAN** (dotted line). TGA were performed under flowing air at a heating rate of 10 ºC·min$^{-1}$ (**Figure S10**); Main data parameters of the MALDI-TOF spectrum of **I-COSAN** (**1**) (**Table S1**); Selected TGA data: residue collected for each analyzed sample at 900 ºC and degree of functionalization of **GO-I-COSAN**. TGA were performed under flowing air at a heating rate of 10 ºC·min$^{-1}$ (**Table S2**).

## AUTHOR INFORMATION

**Corresponding Author**

* E-mail: rosario@icmab.es ; gerard.tobias@icmab.es

**Notes**

The authors declare no competing financial interests.

## Acknowledgements

This work was supported by the Spanish Ministry of Science and Innovation MICINN, through the Severo Ochoa Program for Centers of Excellence FUNFUTURE (CEX2019-000917-S), for funding with an internal Severo Ochoa FIP project. JL thanks the Spanish Ministry of Economy and Competitiveness for funding through Grant CTQ2017-87637-R. Part of the work was conducted under the Maria de Maeztu Units of Excellence Programme – Grant No. MDM-2017-0720. AMJ and AL thanks financial support from the Spanish Ministry of Science and Innovation through the RTI2018-096273-B-I00 project, the PhD scholarship of AMJ (FPU18/05190), and the Generalitat de Catalunya with the projects 2017SGR765 and 2017SGR581. AMJ and AL participated in the MICINN, "Research Networks" nanoCARE, (RED2018-102469-T). The authors thank the staff from the Servei de Cultius Cel·lulars

(SCAC) and the Servei de Microscòpia (SM), both at Universitat Autònoma de Barcelona (UAB), for performing the cytotoxicity studies, the cellular uptake analysis and the HRTEM.

**References**


(1) Smith, B. R.; Gambhir, S. S. Nanomaterials for In Vivo Imaging. *Chem. Rev.* **2017**, *117*, 901−986.

(2) Janib, S. M.; Moses, A. S.; MacKay, J. A. Imaging and Drug Delivery Using Theranostic Nanoparticles. *Adv. Drug Deliv. Rev.* **2010**, *62*, 1052–1063.

(3) Xie, J.; Lee, S.; Chen, X. Nanoparticle-Based Theranostic Agents. *Adv. Drug Deliv. Rev.* **2010**, *62*, 1064–1079.

(4) Cheng, C.; Li, S.; Thomas, A.; Kotov, N. A.; Haag, R. Functional Graphene Nanomaterials Based Architectures: Biointeractions, Fabrications, and Emerging Biological Applications. *Chem. Rev.* **2017**, *117*, 1826−1914.

(5) Sandoval, S.; Kepic, D.; Pérez del Pino, A.; György, E.; Gómez, A.; Pfannmoeller, M.; Van Tendeloo, G.; Ballesteros, B.; Tobias, G. Selective Laser-Assisted Synthesis of Tubular van der Waals Heterostructures of Single-Layered $PbI_2$ within Carbon Nanotubes Exhibiting Carrier Photogeneration. *ACS Nano* **2018**, *12*, 6648-6656.

(6) Weiss, C.; Carriere, M.; Fusco, L.; Capua, I.; Regla-Nava, J. L.; Pasquali, M.; Scott, J. A.; Vitale, F.; Unal, M. A.; Mattevi, C.; Bedognetti, D.; Merkoçi, A.; Tasciotti, E.; Yilmazer, A.; Gogotsi, Y.; Stellacci, F.; Delogu, L. G. Toward Nanotechnology-Enabled Approaches against the COVID-19 Pandemic. *ACS Nano* **2020**, *14*, 6383-6406.

(7) Hong, G.; Diao, S.; Antaris, A. L.; Dai, H. Carbon Nanomaterials for Biological Imaging and Nanomedicinal Therapy. *Chem. Rev.* **2015**, *115*, 10816−10906.

(8) Ji, D-K.; Ménard-Moyon, C.; Bianco, A. Physically-Triggered Nanosystems Based on Two-Dimensional Materials for Cancer Theranostics. *Adv. Drug Deliv. Rev.* **2019**, *138*, 211–232.

(9) Wang, J. T-W.; Klippstein, R.; Martincic, M.; Pach, E.; Feldman, R.; Šefl, Michel, Y.; Asker, D.; Sosabowski, J. K.; Kalbac, M.; Da Ros, T.; Ménard-Moyon, C.; Bianco, A.; Kyriakou, I.; Emfietzoglou, D.; Saccavini, J. C.; M.; Ballesteros, B.; Al-Jamal, K. T.; Tobias, G. Neutron Activated $^{153}$Sm Sealed in Carbon Nanocapsules for in Vivo Imaging and Tumor Radiotherapy. *ACS Nano* **2020**, *14*, 129-141.

(10) Wang, Z.; Ciacchi, L. C.; Wei, G. Recent Advances in the Synthesis of Graphene-Based Nanomaterials for Controlled Drug Delivery. *Appl. Sci.* **2017**, *7*, 1175-1192.

(11) Rodrigues, A. F.; Newman, L.; Jasim, D.; Mukherjee, S. P.; Wang, J.; Vacchi, I. A.; Ménard-Moyon, C.; Bianco, A.; Fadeel, B.; Kostarelos, K.; Bussy, C. Size-Dependent

Pulmonary Impact of Thin Graphene Oxide Sheets in Mice: Toward Safe-by-Design. *Adv. Sci.*, **2020**, *7*, 1903200

(12) Sun, X.; Liu, Z.; Welsher, K.; Robinson, J. T.; Goodwin, A.; Zaric, S.; Dai, H. Nano-graphene Oxide for Cellular Imaging and Drug Delivery. *Nano Res.* **2008**, *1*, 203-212.

(13) Tian, J.; Luo, Y.; Huang, L.; Feng, Y.; Ju, H.; Yu, B. Pegylated Folate and Peptide-Decorated Graphene Oxide Nanovehicle for In Vivo Targeted Delivery of Anticancer Drugs and Therapeutic Self-Monitoring. *Biosens. Bioelectron.* **2016**, *80*, 519-524.

(14) Tadyszak, K.; Wychowaniec, J. K.; Litowczenko, J. Biomedical Applications of Graphene-Based Structures. *Nanomaterials*, **2018**, *8*, 944.

(15) Wong, X. Y.; Sena-Torralba, A.; Álvarez-Diduk, R.; Muthoosamy, K.; Merkoçi, A. Nanomaterials for Nanotheranostics: Tuning Their Properties According to Disease Needs. *ACS Nano* **2020**, *14*, 2585-2627.

(16) Mousavi, S. M.; Hashemi, S. A.; Ghasemi, Y.; Amani, A. M.; Babapoor A.; Arjmand, O. Applications of graphene oxide in case of nanomedicines and nanocarriers for biomolecules: review study. *Drug Metabolism Reviews*, **2019**, *51*, 12-41.

(17) Imani, R.; Mohabatpour, F.; Mostafavi, F. Graphene-based-nano-carriers modifications for gene delivery applications. *Carbon*, **2018**, *140*, 569-591.

(18) Javanbakht, S.; Pooresmaeil, M.; Namazi, H. Green one-pot synthesis of carboxymethylcellulose/Zn-based metal-organic framework/graphene oxide bio-nanocomposite as a nanocarrier for drug delivery system. *Carbohydr. Polym.*, **2019**, *208*, 294-301.

(19) Barahuiea, F.; Saifullaha, B., Dorniania, D.; Fakurazid, S.; Karthivashand, G.; Husseina, M. Z.; Elfghi, F. M. Graphene oxide as a nanocarrier for controlled release and targeteddelivery of an anticancer active agent, chlorogenic acid. *Mat. Sci. Eng. C*, **2017**, *74*, 177-185.

(20) Ghawanmeh, A. A.; Ali, G. A. M.; Algarni, H.; Sarkar, S. M.; Chong, K. F. Graphene oxide-based hydrogels as a nanocarrier for anticancer drug delivery. *Nano Research*, **2019**, *12*, 973-990.

(21) Masalles, C.; Llop, J.; Viñas, C.; Teixidor, F. Extraordinary Overoxidation Resistance Increase in Self-Doped Polypyrroles by Using Non-conventional Low Charge-Density Anions. *Adv. Mater.* **2002**, *14*, 826-829.

(22) Rak, J.; Dejlová, B.; Lampová, H.; Kaplánek, R.; Matějíček, P.; Cígler, P.; Král, V. On the Solubility and Lipophilicity of Metallacarborane Pharmacophores. *Mol. Pharm.* **2013**, *10*, 1751-1759.

(23) Dąbrowska, A.; Matuszewski, M.; Zwoliński, K.; Ignaczak, A.; Olejniczak, A. B. Insight into lipophilicity of deoxyribonucleoside-boron cluster conjugates. *Eur. J. Pharm. Sci.* **2018**, *111*, 226-237.

(24) Grimes, R. N. *Carboranes*, Academic Press, Elsevier, Amsterdam and New York, **2016**.

(25) Housecroft, C. E. *Boron: Metallacarbaboranes, In Encyclopedia of Inorganic and Bioinorganic Chemistry*, John Wiley & Sons, New York, **2011**.

(26) Sivaev, I. B.; Bregadze, V. I. Chemistry of Cobalt Bis(dicarbollides). A Review. *Collect. Czech. Chem. Commun.*, **1999**, *64*, 783-805.

(27) Cabrera-González, J.; Sánchez-Arderiu, V.; Viñas, C.; Parella, T.; Teixidor, F.; Núñez, R. Redox-Active Metallacarborane-Decorated Octasilsesquioxanes. Electrochemical and Thermal Properties. *Inorg. Chem.* **2016**, *55*, 11630–11634.

(28) Gassin, P.-M.; Girard, L.; Martin-Gassin, G.; Brusselle, D.; Jonchère, A.; Diat, O.; Viñas, C.; Teixidor, F.; Bauduin, P. Surface Activity and Molecular Organization of Metallacarboranes at the Air-Water Interface Revealed by Nonlinear Optics. *Langmuir* **2015**, *31*, 2297-2303.

(29) Bauduin, P.; Prevost, S.; Farràs, P.; Teixidor, F.; Diat, O., Zemb, T. A A Theta-Shaped Amphiphilic Cobaltabisdicarbollide Anion: Transition from Monolayer Vesicles to Micelles. *Angew. Chem. Int. Ed.* **2011**, *50*, 5298–5300.

(30) Brusselle, D.; Bauduin, P.; Girard, L.; Zaulet, A.; Viñas, C.; Teixidor, F.; Ly, I.; Diat, O. Lyotropic Lamellar Phase Formed from Monolayered θ-Shaped Carborane-Cage Amphiphiles. *Angew. Chem. Int. Ed.* **2013**, *52*, 12114 –12118.

(31) Uchman, M.; Ďorďovič, V.; Tošner, Z.; Matějíček, P. Classical Amphiphilic Behavior of Nonclassical Amphiphiles: A Comparison of Metallacarborane Self-Assembly with SDS Micellization. *Angew. Chem. Int. Ed.* **2015**, *54*, 14113-14117.

(32) Fernández-Álvarez, R.; Ďorďovič, V.; Uchman, M.; Matějíček, P. Amphiphiles without Head-and-Tail Design: Nanostructures Based on the Self-Assembly of Anionic Boron Cluster Compounds. *Langmuir* **2018**, *34*, 3541-3554.

(33) Malaspina, D. C.; Viñas, C.; Teixidor, F.; Faraudo, J. Atomistic Simulations of COSAN: Amphiphiles without a Head-and-Tail Design Display "Head and Tail" Surfactant Behavior. *Angew. Chem. Int. Ed.* **2020**, *59*, 3088-3092.

(34) Tarrés, M.;. Canetta, E.; Paul, E.; Forbes, J.; Azzouni, K.; Viñas, C.; Teixidor, F.; Harwood, A. Biological Interaction of Living Cells with COSAN-Based Synthetic Vesicles. *Sci. Rep.* **2015**, *5*, 7804. DOI: 10.1038/srep07804

(35) Tarrés, M.; Canetta, E.; Viñas, C.; Teixidor, F.; Harwood, A. J. Imaging in living cells using νB–H Raman spectroscopy: monitoring COSAN uptake. *Chem. Commun.* **2014**, *50*, 3370-3372.

(36) Uchman, M.; Jurkiewicz, P.; Cígler, P.; Grüner, B.; Hof, M.; Procházka, K.; Matějíček, P. Interaction of Fluorescently Substituted Metallacarboranes with Cyclodextrins and Phospholipid Bilayers: Fluorescence and Light Scattering Study. *Langmuir* **2010**, *26*, 6268-6275.

(37) Chaari, M.; Gaztelumendi, N.; Cabrera-González, J.; Peixoto-Moledo, P.; Viñas, C.; Xochitiotzi-Flores, E.; Farfán, N.; Ben Salah, A.; Nogués, C.; Núñez, R. Fluorescent BODIPY-Anionic Boron Cluster Conjugates as Potential Agents for Cell Tracking. *Bioconjugate Chem.* **2018**, *29*, 1763 -1773.

(38) Cabrera-González, J.; Muñoz Flores, B. M.; Viñas, C.; Chávez-Reyes, A.; Dias, H. V. R.; Jiménez Pérez, V. M.; Núñez, R. Organotin Dyes Bearing Anionic Boron Clusters as Cell-Staining Fluorescent Probes. *Chem. Eur. J.* **2018**, 24, 5601 –5612.

(39) Núñez, R.; Juárez-Pérez, E. J.; Teixidor, F.; Santillan, R.; Farfán, N.; Abreu, A.; Yépez, R.; Viñas, C. Decorating Poly(alkyl aryl-ether) Dendrimers with Metallacarboranes. *Inorg. Chem.* **2010**, *49*, 9993-10000.

(40) Cabrera-González, J.; Chaari, M.; Teixidor, F.; Viñas, C.; Núñez, R. Blue Emitting Star-Shaped and Octasilsesquioxane-Based Polyanions Bearing Boron Clusters. Photophysical and Thermal Properties. *Molecules* **2020**, *25*, 1210.

(41) Hao, E.; Zhang, M.; Wenbo, E.; Kadish, K. M.; Froczeck, F. R.; Courtney, B. H.; Vicente, M. G. H. Synthesis and Spectroelectrochemistry of N-Cobaltacarborane Porphyrin Conjugates. *Bioconjugate Chem.* **2008**, *19*, 2171 -2181; and references therein.

(42) Atmaca, G. Y.; Dizman, C.; Eren T.; Erdogmus, A. Novel axially carborane-cage substituted silicon phthalocyanine photosensitizer; synthesis, characterization and photophysicochemical properties. *Spectrochim. Acta, Part A: Molecular and Biomolecular Spectroscopy*. **2015**, *137*, 244-249.

(43) Ďorďovič, V.; Uchman, M.; Reza, M.; Ruokolainen, J.; Zhigunov, A.; Ivankov, O. I.; Matejicek, P. Cation-sensitive compartmentalization in metallacarborane containing polymer nanoparticles. *RSC Adv.* **2016**, *6*, 9884-9892.

(44) Pulagam , K. R.; Gona, K. B.; Gómez-Vallejo, V.; Meijer, J.; Zilberfain, C.; Estrela-Lopis, I.; Baz, Z.; Cossío, U.; Llop, J. Gold Nanoparticles as Boron Carriers for Boron Neutron Capture Therapy: Synthesis, Radiolabelling and In Vivo Evaluation. *Molecules* **2019**, *24*, 3609.

(45) Juárez-Pérez, E. J.; Mutin, P. H.; Granier, M.; Teixidor, F.; Núñez, R. Anchoring of phosphorus-containing cobaltabisdicarbollide derivatives to titania surface. *Langmuir* **2010**, *26*, 12185-12189.

(46) Cabana, L.; González-Campo, A.; Ke, X.; Van Tendeloo, G.; R. Núñez, R.; Tobias, G. Efficient Chemical Modification of Carbon Nanotubes with Metallacarboranes. *Chem. Eur. J.* **2015**, *21*, 16792–16795.

(47) Cabrera-González, J.; Cabana, L.; Ballesteros, B.; Tobias, G.; Núñez, R. Highly Dispersible and Stable Anionic Boron Cluster–Graphene Oxide Nanohybrids. *Chem. Eur. J.* **2016**, *22*, 5096-5101.

(48) Vrbata, D., Ďorďovič, V.; Seitsonen, J.; Ruokolainen, J., Janouskova, O., Uchman, M.; Matejıcek, P. Preparation of membrane-mimicking lamellar structures by molecular confinement of hybrid nanocomposites. *Chem.Commun*., **2019**, *55*, 2900-2903

(49) Leśnikowski, Z. J. Challenges and Opportunities for the Application of Boron Clusters in Drug Design. *J. Med. Chem.* **2016**, *59*, 7738-7758.

(50) Scholz, M.; Hey-Hawkins, E. Carbaboranes as Pharmacophores: Properties, Synthesis, and Application Strategies. *Chem. Rev.* **2011**, *111*, 7035-7062.

(51) Sivaev, I. B.; Bregadze, V. V. Polyhedral Boranes for Medical Applications: Current Status and Perspectives. *Eur. J. Inorg. Chem.* **2009**, 1433-1450.

(52) Fuentes, I.; Garcia-Mendiola, T.; Sato, S.; Pita, M.; Nakamura, H.; Lorenzo, E.; Teixidor, F.; Marques, F.; Viñas, C. Metallacarboranes on the Road to Anticancer Therapies: Cellular Uptake, DNA Interaction, and Biological Evaluation of Cobaltabisdicarbollide [COSAN]$^{-}$. *Chem. Eur. J.* **2018**, *24*, 17239-17254.

(53) Couto, M.; Alamón, C.; García, M. F.; Kovacs, M.; Trias, E.; Nievas, S.; Pozzi, E.; Curotto, P.; Thorp, S.; Dagrosa, M.A.; Texidor, F.; Viñas, C.; Cerecetto, H. Closo-Carboranyl- and Metallacarboranyl[1,2,3]triazolyl-Decorated Lapatinib-Scaffold forCancer Therapy Combining Tyrosine KinaseInhibition and Boron Neutron Capture Therapy. *Cells*, **2020**, *9*, 1408; doi:10.3390/cells9061408.

(54) Xuan, S.; Vicente, M. G. H., *Recent Advances in Boron Delivery Agents for Boron Neutron Capture Therapy (BNCT). In Boron-based Compounds: Potential and Emerging Applications in Biomedicine (Eds. Hey-Hawkins E. and Viñas, C.)*, John Wiley & Sons, Hoboken (NJ), **2018**, pp. 298-342.

(55) Barth, R. F.; Mi, P.; Yang, W. A realistic appraisal of boron neutron capture therapy as a cancer treatment modality. *Cancer Commun.* **2018**, *38*, article number 35 and references therein.

(56) Hu, K.; Yang, Z.; Zhang, Xie, L.; Wang, L.; Xu, H.; Josephson, L.; Liang, S. H.; Zhang, M.-R. Boron agents for neutron capture therapy. *Coord. Chem. Rev.* **2020**, *405*, 213139.

(57) Li, J.; Fernandez-Alvarez, R.; Kereïche, S.; Uchman, M.; Matejicek, P. Designed Boron-Rich Polymeric Nanoparticles Based on Nano- Ion Pairing for Boron Delivery. *Chem. Eur. J*., **2020**; *26*,14283 –14289.

(58) Gona, K. B.; Zaulet, A.; Gómez-Vallejo, V.; Teixidor, F.; Llop, J.; Viñas, C. COSAN as a molecular imaging platform: synthesis and "in vivo" imaging. *Chem. Commun.* **2014**, *50*, 11415-11417.

(59) Sivaev, I. B.; Starikova, Z. A.; Sjöberg, S.; Bregadze,V. I. Synthesis of functional derivatives of the $[3,3'\text{-}Co(1,2\text{-}C_2B_9H_{11})_2]^-$ anion. *J. Organomet. Chem.* **2002**, *649*, 1–8.

(60) Leites, L. A. Vibrational spectroscopy of carboranes and parent boranes and its capabilities in carborane chemistry. *Chem. Rev*., **1992**, *92*, 279-323.

(61) Sandoval, S.; Kumar, N.; Oro-Solé, J.; Sundaresan, A.; Rao, C. N. R.; Fuertes, A.; Tobias, G. Tuning the nature of nitrogen atoms in N-containing reduced graphene oxide. *Carbon* **2016**, *96*, 594-602.

(62) Worle-Knirsch, J. M.; Pulskamp, K.; Krug, H. F. Oops They Did It Again! Carbon Nanotubes Hoax Scientists in Viability Assays. *Nano Lett.* **2006**, *6*, 1261-1268.

(63) Ali-Boucetta, H.; Al-Jamal, K. T.; Kostarelos, K. Cytotoxic assessment of carbon nanotube interaction with cell cultures. *Methods Mol. Biol.* **2011**, *726*, 299-312.

(64) Goszczyński, T. M.; Fink, K.; Kowalski, K.; Leśnikowski, Z. J.; Boratyński, J. Interactions of Boron Clusters and their Derivatives with Serum Albumin. *Sci. Rep.* **2017**, *7*, 9800.

(65) Fuentes, I.; Pujols, J.; Viñas, C.; Ventura, S.; Teixidor, F. Dual Binding Mode of Metallacarborane Produces a Robust Shield on Proteins. *Chem. Eur. J*. **2019**, *25*, 12820-12829.

(66) Llop, J. Jiang, P.; Marradi, M.; Gómez-Vallejo, V.; Echeverría. M.; Yu, S.; Puigivila, M.; Baz, Z.; Szczupak, B.; Pérez-Campaña, C.; Mao, Z.; Gao, C.; Moya, S. E. Visualisation of dual radiolabelled poly(lactide-co-glycolide) nanoparticle degradationin vivousingenergy-discriminant SPECT. *J. Mater. Chem. B*, **2015**, *3*, 6293-6300.

(67) a) Semioshkin, A.; Nizhnik, E.; Godovikov, I.; Starikova, Z.; Bregadze, V. Reactions of oxonium derivatives of $[B_{12}H_{12}]^{2-}$ with amines: Synthesis and structure of novel B12-based ammonium salts and amino acids. *J. Organomet. Chem.* **2007**, *692*, 4020–4028.

(68) Brenner, S. The genetics of Caenorhabditis elegans. *Genetics* **1974**, *77*, 71–94.
(69) González-Moragas, L.; Yu, S. M.; Carenza, E.; Laromaine, A.; Roig, A. Protective Effects of Bovine Serum Albumin on Superparamagnetic Iron Oxide Nanoparticles Evaluated in the Nematode Caenorhabditis elegans. *ACS Biomater. Sci. Eng.* **2015**, *1*, 1129–1138.
(70) Sramkova, M.; Kozics, K.; Masanova, V.; Uhnakova, I.; Razga, F.; Nemethova, V.; Mazancova, P.; Kapka-Skrzypczak, L.; Kruszewski, M.; Novotova, M.; Puntes, V. F.; Gabelova. A. Kidney nanotoxicity studied in human renal proximal tubule epithelial cell line TH1. *Mutat. Res. Gen. Tox. En*. **2019**, *845*, 403017.

## TOC Graphic

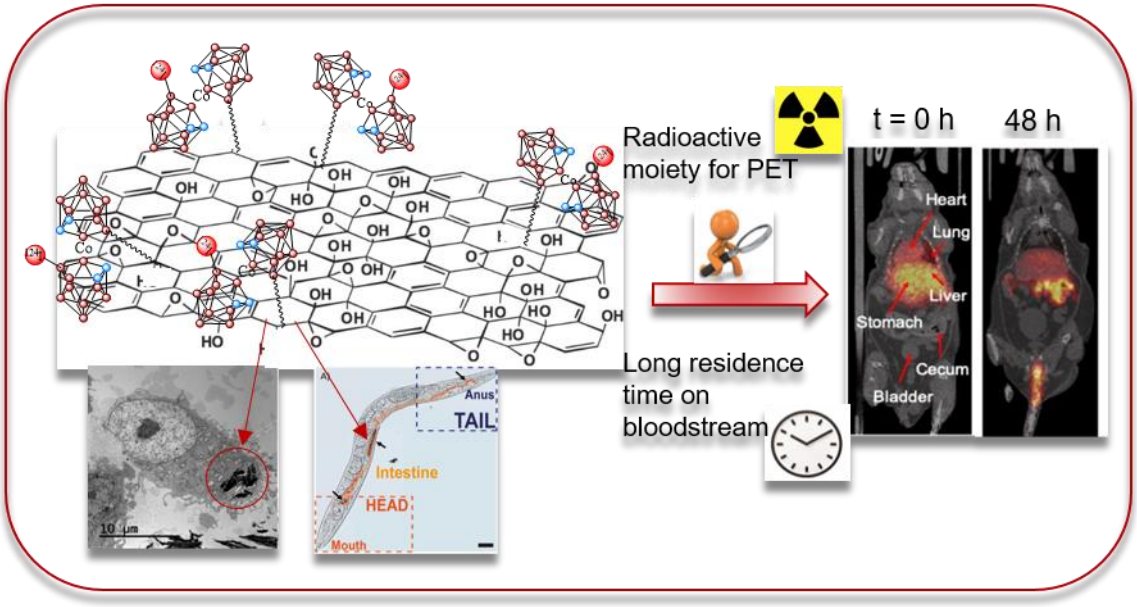


Radiolabeled Cobaltabisdicarbollide Anion-Graphene Oxide Nanocomposites for In-Vivo Bioimaging and Boron Delivery